Journal of Alloys and Compounds, Volume 549, 5 February 2013, Pages 283–287

Dielectric tunability properties of the $Pb(Mg_{1/3}Nb_{2/3})_{0.8}(Sc_{1/2}Nb_{1/2})_{0.2}O_3$ ceramics

Biaolin Peng[1], Huiqing Fan[1, a)], Qi Zhang[2]

[1]State Key Laboratory of Solidification Processing, School of Materials Science and Engineering, Northwestern Polytechnical University, Xi'an 710072, China

[2]Department of Materials, Cranfield University, Cranfield, Bedfordshire, MK43 0AL, United Kingdom

Abstract

Pure perovskite $Pb(Mg_{1/3}Nb_{2/3})_{0.8}(Sc_{1/2}Nb_{1/2})_{0.2}O_3$ ceramics was prepared via a modified "columbite-type" method. The 1:1 B-site ordered structure of $Pb(Sc_{1/2}Nb_{1/2})O_3$ was detected by XRD and TEM. The dielectric relaxor behavior was described by a Lorentz relation. The dielectric tunability properties were investigated at 300K and 10 kHz. The results show that the ceramics possesses high dielectric tunability (~ 75% at 30 kV/cm), low dielectric loss (~ 0.003) and high figure of merit (~ 250), indicating that it is a promising tunable material. The high dielectric nonlinear behavior was illustrated by employing the Landau-Ginsberg-Devonshire thermodynamic theory and a multipolarization mechanism model. The results indicate that the high non-linearity is related to the contributions of the "extrinsic" polarizations such as the polar nanoregions and nanometer domain wall motions, etc., in addition to the contribution of the "intrinsic" lattice phonon polarization.

[a)] Corresponding author, E-mail: hqfan3@163.com, Tel: +86-29-88494463, Fax: +86-29-88492642

1. Introduction

Recently, there has been considerable interest in electric field tunable dielectric materials due to their potential applications as phase shifters, filters, and wireless communications[1-3]. These applications demand dielectric materials possessing high dielectric tunability, low dielectric loss and thermal stability [4,5], etc. However, it was found that the high dielectric tunability and low dielectric loss are two conflicting parameters; high dielectric tunability generally leads to high dielectric loss. Usually, an effective way to get the best compromise between the two is to dope oxides that have low dielectric losses, such as MgO, ZrO_2, Al_2O_3, TiO_2 and $MgAl_2O_4$[6-10], etc., into the dielectric materials. To attain these requirements, most research efforts in this field are focused on investigating normal ferroelectrics $(Ba,Sr)TiO_3$, $(Ba,Sn)TiO_3$, and $(Sr,Pb)TiO_3$ system[], etc. Other possible candidates for such applications are relaxor ferroelectrics, such as $Ba(Zr,Ti)O_3$, $Ba(Ti,Ga,Nb)O_3$, $(Pb,Ba,La)(Zr,Sn,Ti)O_3$ and PMN[], etc, which are characterized by a broad and frequency-dependent relative permittivity maximum ($\varepsilon_{r,max}$)[].

The $Pb(Sc_{1/2}Nb_{1/2})O_3$ (PSN) ceramics exhibits normal ferroelectric behavior due to the formation of a complete 1:1 B-site ordered structure, in which one cation position occupied by scandium and the other by niobium[]. In contrast, the $Pb(Mg_{1/3}Nb_{2/3})O_3$ (PMN) ceramics exhibits prototypical relaxor ferroelectric behavior. The difference is attributed to the absence of complete chemical order in the 1:1 random site of the PMN systems[]. One interesting thing is that complete 1:1 B-site ordering can be induced in the PMN relaxor ferroelectric by a small amount of B-site

additives such as Sc, etc[]. As a result, in the $Pb(Mg_{1/3}Nb_{2/3})_{1-x}(Sc_{1/2}Nb_{1/2})_xO_3$ (PSMN) systems, a crossover from relaxor to normal ferroelectric behavior can be observed close to x = 0.5. However, up to now, to our knowledge, literatures concerning the tunable dielectric properties of the PSMN ceramics are rare. Therefore, it is quite necessary to carry out the investigations on the aforementioned topics.

In this work, we report the dielectric tunability properties of the $Pb(Mg_{1/3}Nb_{2/3})_{0.8}(Sc_{1/2}Nb_{1/2})_{0.2}O_3$ (PSMN20) ceramics possessing B-site cation 1:1 partially-ordering at room temperature. It is found that high dielectric tunability, low dielectric loss and high figure of merit can be achieved in this composition.

2. Experimental procedure

The PSMN20 ceramics were synthesized using high-purity (99.9%) oxides via a modified "columbite-type" route[]. Firstly, analytical grade powders of the B-site oxides were pre-reacted at 1100 °C for 6 h in air, and then the pre-reacted powders were mixed with stoichiometric amounts of lead oxide powders, milled for 6 h and calcined at 900 °C for 4 h to form perovskite phase. Pressed pellets, with 10 mm in diameter by 1 mm thick, were formed by cold-isostatic pressing at 300 MPa. The preformed pellets were sintered at 1240 °C for 2 h in air and then cooled naturally to room temperature. Sintering was carried out inside a covered alumina crucible, and the pellets were covered with powder of the same composition to minimize the lead loss during firing.

The density of all the pellets was measured by the Archimedes method. The crystal structures of the sintered pellets were analyzed using X-ray diffraction (XRD;

D/Max2550VB+/PC, Rigaku, Tokyo, Japan) with Cu K_α radiation (λ = 0.15406 nm) over 2θ in the range of 10º-90º. The crystal phases were compared with the powder diffraction data from JCPDS-ICDD (International Center of Diffraction Data). The microstructure of the ceramics was characterized using field emission transmission electron microscope (TEM; Tecnai F30G^2, FEI, America) operated at 300 kV.

Low-field dielectric responses at a signal level of 500 mV/mm were measured by using a precision impedance analyzer (4294A, Agilent, USA) associated with a temperature controller (TP94, Linkam, UK) over a temperature range of 173–673 K at a heating rate of 3 °C/min. The dc electric field dependence of the dielectric permittivity was measured at 10 kHz and 300 K.

3. Results and discussions

Density measurement indicates that the PSMN20 ceramics has relative density 98%. X-ray diffraction (XRD) pattern (Fig. 1) indicates that single perovskite phase composition with a cubic symmetry (unit cell parameter a = 4.082 Å) was formed. Weak superlattice diffractions were detected, indicating the formation of a 1:1 B-site ordered structure []. The appearance of ordered domains (see the inset in Fig. 1) in the TEM centered dark-field image (CDF) formed with the $\left(\frac{1}{2}\frac{1}{2}\frac{1}{2}\right)$ superlattice spot in the <110> zone axis electron diffraction pattern, further confirms the existence of 1:1 B-site ordered structure. Obviously, it is a partial 1:1 B-site ordered structure for PSMN20. In addition, the sharp electron diffraction spots with no satellites also further confirm the existence of single perovskite phase.

The dependence of the real part (ε') and imaginary part (ε'') of dielectric

permittivity vs. temperature at 100 Hz, 1 kHz and 10 kHz is shown in Fig. 2. The dielectric properties show high values of the real part of permittivity at room temperature and 10 kHz (~10,000) and at T_m (~12,000); and low imaginary part: $\varepsilon'' <$ 0.03 in the range (300–600)K and below 0.5 at T_m. The PSMN20 ceramics exhibits typical relaxor character, namely the decrease of T_m at the maximum $\varepsilon'(T)$ with the increase of frequency and the strong dielectric dispersion at temperatures around and below T_m, or the increase of $T_{m''}$ at the maximum $\varepsilon''(T)$ maximum with the increase of frequency and the strong dielectric dispersion at temperatures around and up $T_{m''}$[]. The relaxor behavior is considered to be closely related to the response of polar nanoregions (PNRs), which are described as nanosized polar islands embedded in an average cubic matrix[].

In order to describe the dielectric relaxor behavior at $T > T_m$, several relations have been proposed, one of which is the Lorentz-type empirical relation[],

$$\varepsilon_A / \varepsilon' = 1 + (T - T_A)^2 / 2\delta_A^2 \qquad (1)$$

Where T_A ($T_A \neq T_m$) and ε_A are the parameters defining the temperature of the dielectric peak and the extrapolated value of ε' at $T = T_A$, respectively. The parameter δ_A is temperature and frequency independent, reflecting the diffuseness of the dielectric peak. The greater the relaxor dispersion is, the bigger δ_A is. It is found that the above relation can describe the high temperature ($T > T_m$) dielectric permittivity quite well in a number of relaxor ferroelectrics[], as well as the normal ferroelectrics such as the $BaTiO_3$[], etc.. Likewise, at $T > T_m$, the $\varepsilon'(T)$ of PSMN20 ceramics can well be fitted by the Lorentz relation (see the red solid line in Fig. 2). Table I lists the

best Lorentz fitting parameters for PSMN20, $Pb(Mg_{1/3}Nb_{2/3})O_3$, $Ba(Zr_{0.25}Ti_{0.75})O_3$ and $BaTiO_3$[]. The $Pb(Mg_{1/3}Nb_{2/3})O_3$, $Ba(Zr_{0.25}Ti_{0.75})O_3$ and $BaTiO_3$ are the classical relaxors, quasi-ferroelectric and normal ferroelectrics[], respectively. The δ_A for PSMN20, $Pb(Mg_{1/3}Nb_{2/3})O_3$, $Ba(Zr_{0.25}Ti_{0.75})O_3$ and $BaTiO_3$ is 77.35, 103.6, 72 and 37, respectively. It can be seen that the δ_A (77.35) for PSMN20 is close to that (72) for $Ba(Zr_{0.25}Ti_{0.75})O_3$. Therefore, it is suggested that a decrease in the degree of relaxor dispersion or an increase in the degree of the order is attained for PSMN20. The result is consistent with that observed in the inset of Fig.1.

Fig. 3 illustrates the temperature dependence of the dielectric loss ($\tan\delta$) of the PSMN20 ceramics at 100 Hz, 1 kHz and 10 kHz. The dielectric loss of the PSMN20 ceramics at 100 Hz, 1 kHz and 10 kHz at 300 K is 0.0025, 0.0027 and 0.003, respectively. Further, low dielectric losses (< 0.005) in a wide temperature (300-400 K) are observed. These results show that the thermal and frequency stabilities, which are important parameters for tunable application, are excellent for PSMN20.

In addition, as shown by the arrow in Fig. 3, there is a low-frequency dielectric relaxation in the higher temperature range (＞ 475 K) . It is reported that an increase in vacancies will lead to an increase in both the conductivity and the dielectric relaxation, as a result, a correlation between the dielectric relaxation and the dc conductivity (σ_{dc}) was established[]. The inset in Fig. 3 shows the $\ln(\sigma_{dc})$ versus 1000/T, the plot is found to be linear and fitted using following Arrhenius equation:

$$\sigma_{dc} = \sigma_0 \exp\{-E_{dc}/(k_B T)\} \quad (2)$$

Where σ_0 is the pre-exponential factor, E_{dc} is the activation energy for the dc

conduction, k_B the Boltzmann constant, and T the absolute temperature. The calculated activation energy was 1.22 eV, which is in good agreement with the activation energy (1.07–1.31 eV) obtained for oxygen vacancies in the perovskite materials[]. Hence, it is reasonable to assume that the localized oxygen vacancies act as "polarons"[], leading to a low frequency dielectric relaxation in the higher temperature range of the dielectric loss.

Fig. 4 shows the dependence of the dielectric permittivity ε' and the dielectric loss $\tan\delta$ vs. dc bias electric field at 10 kHz and 300 K. It can be seen that the dielectric permittivity ε' decreases sharply with the increase of the electric field, indicating that there is a high dielectric nonlinear electric field dependence, whilst the dielectric loss decreases slightly with the increase of the electric field. The dielectric tunability (η_r) was defined as:

$$\eta_r(\%) = \frac{(\varepsilon'(0) - \varepsilon'(E))}{\varepsilon'(0)} \times 100 \quad (3)$$

where $\varepsilon'(0)$ and $\varepsilon'(E)$ represent the real part of the dielectric permittivity at zero and applied electric field, respectively. It was found that the dielectric tunability increases with the increase of the electric field and the large value of 75% is obtained at E = 30 kV/cm. Nonetheless, the competence of a dielectric for tunable applications requires not only high value of dielectric tunability but also low dielectric loss. Figure-of-merit (*FOM*) of dielectric tunable properties is defined as:

$$FOM = \frac{\eta_r(\%)}{\tan\delta_0} \quad (4)$$

where tanδ_0 is the dielectric loss without dc bias. Similar to the dielectric tunability, *FOM* obtained in the PSMN20 ceramics also increases with the increase of the electric field and a maximum value of 250 appears at E = 30 kV/cm. For comparison, Table II lists the *FOMs* for the PSMN20, $Ba_{0.4}Sr_{0.6}TiO3$, $BaZr_{0.30}Ti_{0.70}O_3$ and $Pb_{0.35}Sr_{0.65}TiO_3$ ceramics respectively[], as well as the η_r and tanδ. The *FOMs* obtained for PSMN20, $Ba_{0.4}Sr_{0.6}TiO3$, $BaZr_{0.30}Ti_{0.70}O_3$ and $Pb_{0.35}Sr_{0.65}TiO_3$ are 250 (30 kV/cm), 200 (30 kV/cm), 225 (40 kV/cm) and 60 (40 kV/cm), respectively, at 10 kHz and 300 K. Obviously, the PSMN20 ceramic has the biggest *FOM*, indicating that it is an attractive material for tunable applications. Furthermore, the higher *FOMs* for this composition may be obtained by further decreasing the dielectric loss through the addition of additives[].

In the case of a single lattice phonon polarization mechanism dominantly existing in polar dielectrics such as $KTaO_3$ and (Sr,Ba)TiO_3[], etc., it is found that the Landau-Ginzburg-Devonshire (LGD) thermodynamic theory works well when describing the $\varepsilon'(E)$. Similarly, in this work, the LGD thermodynamic theory is employed to analyze the $\varepsilon'(E)$ of PSMN20.

$$\varepsilon'(E) = \varepsilon'(0)/\{1 + \lambda[\varepsilon_0 \varepsilon'(0)^3 E^2]\}^{1/3} \quad (5)$$

where ε_0 is the permittivity of free space, λ is a temperature-independent coefficient. The blue short dot line in Fig.4 shows the fitting of the Eq. (5) to the $\varepsilon'(E)$ of PSMN20 at 10 kHz and 300 K. Obviously, LGD is invalid for describing the $\varepsilon'(E)$. It has been known that, for relaxor ferroelectrics, in addition to the "intrinsic" contribution such as electron and phonon, the "extrinsic" contribution such as the nanopolar clusters (or

polar nanoregions), domain wall motions and domain boundary polarization may become important at low frequencies[]. Therefore, it is not hard to understand the unavailability for the LGD describing the $\varepsilon'(E)$ of PSMN20.

Taking into account of the contribution of the "intrinsic" and "extrinsic" polarizations to the $\varepsilon'(E)$, a multipolarization mechanism model is applied for the PSMN20 relaxor ferroelectric[].

$$\varepsilon(E) = \varepsilon_r(0)/\{1 + \lambda[\varepsilon_0\varepsilon_r(0)^3 E^2]\}^{1/3} + (P_r x/\varepsilon_0)[\cosh(Ex)]^{-2} \quad (6)$$

where the first term represents the "intrinsic" polarization, the latter represents the "extrinsic" polarization contribution. The P_r is the effective polarization of one cluster, V the cluster size and k_B Boltzmann's constant and $x = P_r V/(k_B T)$. It can be seen that the experiment data is in good agreement with the multipolarization mechanism model (see the red solid line in Fig. 4). The result indicates that the high dielectric nonlinear behavior of the PSMN20 ceramics is related to the "extrinsic" polarization, in addition to the contribution of the "insinsic" lattice phonon polarization.

4. Conclusions

Pure perovskite $Pb(Mg_{1/3}Nb_{2/3})_{0.8}(Sc_{1/2}Nb_{1/2})_{0.2}O_3$ relaxor ferroelectric ceramics can be synthesized using a modified "columbite-type" method. The partially-ordered 1: 1 B-site cation structure of was achieved. The high dielectric tunability (~ 75% at 30 kV/cm), low dielectric loss (~ 0.003) and high figure of merit (~ 250) were observed at 10 kHz and 300 K, making it become an attractive material for tunable device applications. The high dielectric nonlinear behavior is related to the contributions of the "extrinsic" polarizations such as the polar nanoregions and

nanometer domain wall motions, etc., in addition to the contribution of the “intrinsic” lattice phonon polarization.

Acknowledgements

This work was supported by the National Nature Science Foundation (51172187), the SPDRF and 111 Program (B08040) of MOE, the Xi’an Science and Technology Foundation (XA-AM-201003), the Fundamental Research Foundation (NPU-FFR-200703) and the SKLSP Research Fund (40-QZ-2009) of China.

References

Captions

Fig.1. XRD patterns of the $Pb(Mg_{1/3}Nb_{2/3})_{0.8}(Sc_{1/2}Nb_{1/2})_{0.2}O_3$ ceramics. The inset is the TEM centered dark-field imaging with the $\left(\frac{1}{2}\frac{1}{2}\frac{1}{2}\right)$ superlattice spot in the <110> zone axis electron diffraction pattern.

Fig.2. The temperature dependence of the real ε' and imaginary ε'' parts of dielectric permittivity of the $Pb(Mg_{1/3}Nb_{2/3})_{0.8}(Sc_{1/2}Nb_{1/2})_{0.2}O_3$ ceramics at 100 Hz, 1 kHz and 10 KHz. The red solid line is the Lorentz fit curve.

Fig.3. The temperature dependence of the dielectric loss ($\tan\delta$) of the $Pb(Mg_{1/3}Nb_{2/3})_{0.8}(Sc_{1/2}Nb_{1/2})_{0.2}O_3$ ceramics at 100 Hz, 1 kHz and 10 KHz. The inset is the temperature dependence of the dc conductivity (σ_{dc}).

Fig.4. The dc electric field dependence of the dielectric permittivity ε' and loss $\tan\delta$ of the $Pb(Mg_{1/3}Nb_{2/3})_{0.8}(Sc_{1/2}Nb_{1/2})_{0.2}O_3$ ceramics at 10 kHz and 300K. The red solid line is the $\varepsilon(E) = \varepsilon_r(0)/\{1+\lambda[\varepsilon_0\varepsilon_r(0)^3E^2]\}^{1/3} + (P_r x/\varepsilon_0)\times[\cosh(Ex)]^{-2}$ and the $\varepsilon(E) = \varepsilon_r(0)/\{1+\lambda[\varepsilon_0\varepsilon_r(0)^3E^2]\}^{1/3}$ fit curves, respectively.

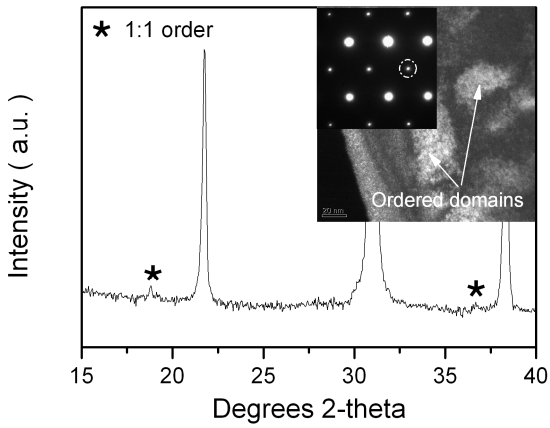

Fig. 1

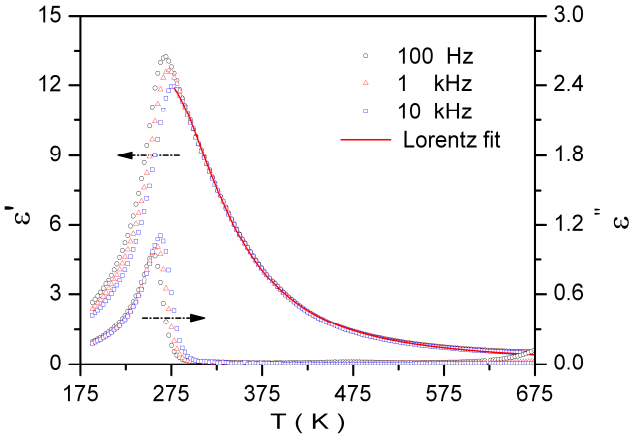

Fig. 2

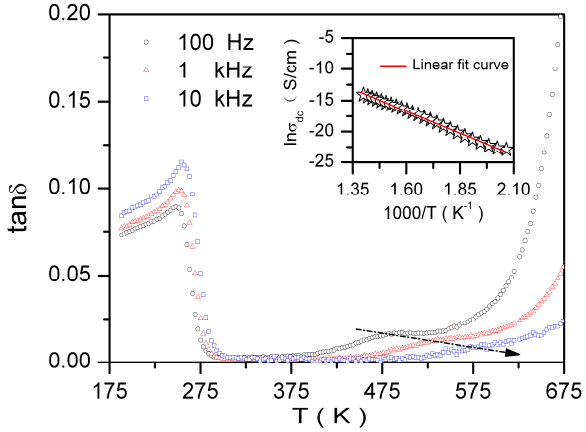

Fig. 3

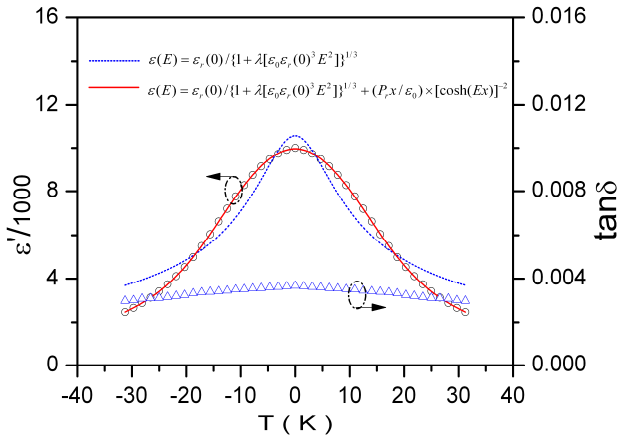
16
12
8
4
0
0.016
0.012
0.008
0.004
0.000
ε'/1000
tanδ
-40
-30
-20
-10
0
10
20
30
40
T (K)
$\varepsilon(E)=\varepsilon_r(0)/\{1+\lambda[\varepsilon_0\varepsilon_r(0)^3E^2]\}^{1/3}$
$\varepsilon(E)=\varepsilon_r(0)/\{1+\lambda[\varepsilon_0\varepsilon_r(0)^3E^2]\}^{1/3}+(P_r x/\varepsilon_0)\times[\cosh(Ex)]^{-2}$

Fig. 4

Table I. Lorentz fit results for $Pb(Mg_{1/3}Nb_{2/3})_{0.8}(Sc_{1/2}Nb_{1/2})_{0.2}O_3$, $Pb(Mg_{1/3}Nb_{2/3})O_3$, $Ba(Zr_{0.25}Ti_{0.75})O_3$ and $BaTiO_3$.

Sample	f (kHz)	T_m (K)	ε_m	T_A （K）	ε_A	δ_A (K）
$Pb(Mg_{1/3}Nb_{2/3})O_3$	10	267.7	10986	250.6	11954	103.6
$Pb(Mg_{1/3}Nb_{2/3})_{0.8}(Sc_{1/2}Nb_{1/2})_{0.2}O_3$	10	281.15	11941	264.28	12257	77.35
$Ba(Zr_{0.25}Ti_{0.75})O_3$	10	232.5	6474	233.3	6364	72
$BaTiO_3$	10	393	23371	358	61670	37

Table II. Dilectric tunabilities (η_r), dielectric losses (tanδ) and figures of merit (*FOM*) for the $Pb(Mg_{1/3}Nb_{2/3})_{0.8}(Sc_{1/2}Nb_{1/2})_{0.2}O_3$, $Ba_{0.4}Sr_{0.6}TiO3$, $BaZr_{0.30}Ti_{0.70}O_3$ and $Pb_{0.35}Sr_{0.65}TiO_3$ at 300 K.

Sample	F (kHz)	E (kV/cm)	η_r	tanδ	*FOM*
$Pb(Mg_{1/3}Nb_{2/3})_{0.8}(Sc_{1/2}Nb_{1/2})_{0.2}O_3$	10	30	75%	0.003	250
$Ba_{0.4}Sr_{0.6}TiO_3$	10	30	12%	0.0006	200
$BaZr_{0.30}Ti_{0.70}O_3$	10	40	45%	0.002	225
$Pb_{0.35}Sr_{0.65}TiO_3$	10	40	48%	0.008	60